

# NEAR-WALL TURBULENCE-BUBBLES INTERACTIONS IN A CHANNEL FLOW AT $Re_\tau=400$ : A DNS/LES INVESTIGATION

D. Métrailler, S. Reboux and D. Lakehal

ASCOMP GmbH, Zurich, Technoparkstr. 1, Switzerland

Metrailler@ascomp.ch; Reboux@ascomp.ch; Lakehal@ascomp.ch

## ABSTRACT

This paper presents results of a Large-Eddy Simulation (LES) of a two-phase air—water mixture in a convective channel flow at  $Re_\tau=400$  using the CFD code TransAT. The aim of this work is to understand the effects of inertial turbulence in convective boiling flow. Thermal effects, nucleation and phase-change are taken into account in companion papers. The interactions between the bubbles and the liquid were studied through an in-depth analysis of the turbulence statistics. The near-wall flow is affected by the bubbles, which act like roughness elements. The coherent structures are different in shape than in single-phase flow, featuring less elongated, broken structures. The decay in the energy spectra near the wall was found to be significantly slower (slope of -3) for the bubbly flow than for a single-phase flow (slope of -6). The database generated is of sufficient quality to extract time-, space- and phase-averaged quantities, thus paving the way for model upscaling and accurate closure models for near-wall bubbly flow simulations using the mixture formulation.

## KEYWORDS

Interface Tracking, turbulence, LES, DNS, bubbly flow

## 1. INTRODUCTION

The prediction of critical heat flux (CHF) conditions is vital in many industrial systems. In pressurized nuclear power reactors, CHF is a kind of limit parameter of operation; therefore its accurate prediction is important both from safety and economic point of views. In the last decade, considerable efforts have been made to use computational fluid dynamics (CFD) methods for the prediction of CHF. The limited success of these attempts motivates more work on the side of modeling. To support the modeling efforts we need reliable and accurate measurements, which are dedicated for development and validation of CFD methods. Beside complex CHF measurements, separate effect tests can be used to develop particulate models relevant in complex CHF modeling. In the development of CHF all transport mechanisms such as mass, momentum and energy transfer play important role.

In the PWR hot channel, beyond the onset of nucleate boiling but before the point of net vapor generation, small vapor bubbles are attached to the fuel rods. Heat and mass are transferred by evaporation from the base to the tip of the bubbles where condensation occurs; therefore, the heat transfer coefficient increases with respect to single-phase flow conditions. Also, the bubbles, effectively, act as surface roughness and thus, depending on their size, may affect the friction coefficient and ultimately the flow distribution across the sub-channels within the fuel assembly. Here the focus is on the effect of the departing bubbles on turbulence characteristics, time-average profiles of the fluid flow, and other global parameters including friction coefficient, pressure drop, etc. Heat transfer and phase change are not part of this benchmark; we only seed bubbles in the channel, as described below.

The aim of these simulations is to demonstrate that the methods applied here are able to predict the major characteristics of bubbly channel flow (bubble clustering, steepening of the rms of the mean velocity etc.). Furthermore, these simulations provide information for higher-level modeling. In particular, a method for

the extraction of *a priori* subgrid-scale stress and surface tension information for the LEIS simulations will be worked out and a database has been generated for further RANS model development. DNS/LES of convective boiling in a channel – a work from the MIT was selected [1]. The schematic of the experimental setup is shown in Figure 1.

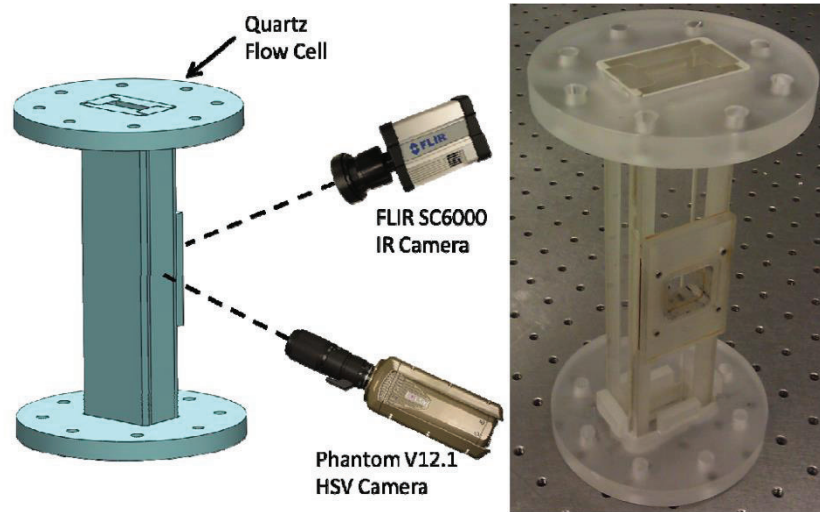


**Figure 1: Exp. setup for HSV and IR thermography (left), picture of the quartz section (right) [1].**

High-Speed Video (HSV) and Infrared (IR) thermography were used to report bubble departure diameter, and IR thermography allowed measurement of wall superheat (local distribution and surface-averaged), heat transfer coefficient, nucleation site density, and bubble wait time. The tests were performed at atmospheric pressure at a constant subcooling of 10°C.

## 2. PROBLEM SETUP

### 2.1 Computational domain, boundary conditions & mesh

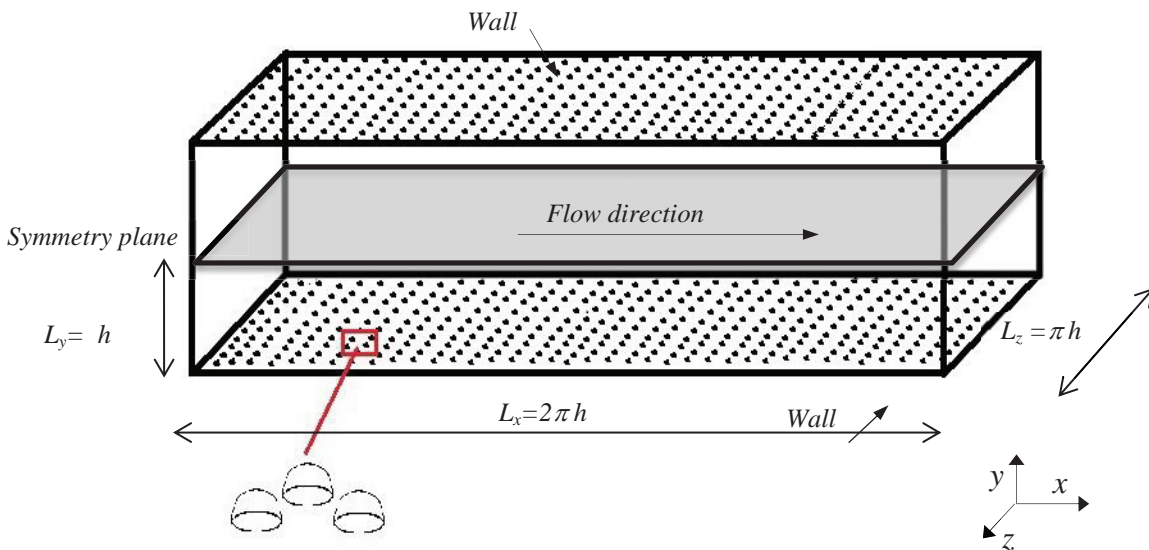


**Figure 2: Computational domain for the benchmark case**

The simulation domain and size are shown in Figure 2. The domain consists of a channel with small hemispherical bubbles attached to the upper and lower walls, representing the bubbles attached to the PWR fuel rods. Several simplifications with respect to the true situation have to be introduced to facilitate the simulations. First, since the bubble diameter is small compared to the channel width, the effect of rod curvature can be neglected, thus a configuration of turbulent flow over a flat wall is justified. Second, since the shear Reynolds number for PWR is  $Re_\tau \sim 10^4$ , performing a DNS or LES for such high  $Re_\tau$  is computationally prohibitive. As such, the benchmark problem is scaled down to more reasonable flow conditions, namely  $Re_\tau = 400$ , for which both DNS and LES simulations are feasible, with possible comparison of the results to existing DNS databases for single-phase flow over rough surfaces at the exact same flow conditions ([2], [3]). In contrast to the original benchmark defined by Chatzikiyiakou et al. [4], in which the bubbles are treated as *solid* hemispherical obstacles adhering to the wall, here the bubbles are allowed to deform, detach and be transported with the flow.

A symmetry boundary condition was used at half channel height (see Figure 2) to reduce computational effort. Periodic boundary conditions were used in the streamwise and spanwise directions. The bubble radius  $r_b$  is chosen to be 0.125 mm, which corresponds to the departure size observed in the experimental conditions. To be consistent with the work of Chatzikiyiakou [4] the normalized bubble radius  $k^+ = u_\tau / \nu r_b$  is chosen to be equal to 10. Using interface tracking for the dispersed phase requires a relatively fine mesh in all directions. A grid spacing of 8 cells for one bubble diameter was found to be sufficient, yielding the normalized grid spacing:

$$\Delta h_f^+ = \Delta x_f^+ = \Delta y_f^+ = \Delta z_f^+ = 2.5.$$

A block mesh refinement (BMR) technique is used to coarsen the grid by a factor 2 away from the wall (for  $y^+$  larger than 90). This leads to approximately 30 million grid cells, distributed in 1'134 blocks. The load balancing is satisfactory, with each block having between 20'000 and 25'000 cubical-shaped cells. The first grid point is at  $y^+ = 1$ , which is inside the viscous sublayer.

## 2.2 Initial conditions

The initial flow conditions for the full domain were generated using cyclic inflow-outflow. During this process, to speed up the turbulent flow generation, various grids of different refinements (coarse, medium and refined) were employed in a sequential way: the solution obtained on the coarse grid is mapped into the medium one, the solution of which is then passed to the fine mesh, which at the end is transferred to the final run as an initial/inflow/outflow condition. Assuming the flow to be non-homogenous with a dominant velocity fluctuation in the flow direction, component  $w'$  (in the flow direction) fixed as the variance of  $u$ . The other components were defined as  $u' = 2/3w'$  and  $v' = 1/3u'$ . This process is innovative; it allows generating the fluctuating field to the finest mesh rather fast.

Once turbulence is fully developed, 557 bubbles with a diameter of 0.25 mm are introduced. Their effect on the flow statistics is studied. Variables such as mean liquid velocity and Reynolds stresses are shown. The dynamics of the bubbles are also analyzed.

## 2.3 Simulations parameters

The simulations were performed on HLRS's supercomputer Hermit, using 1134 MPI cores. For the single-phase simulation, flow averaging started at 89,852 time steps, with 10,000 additional steps to infer ergodic conditions, achieving around 4 flow-through times. In the two-phase simulation, a total of 120,000 iterations were performed. Because the interface tracking method requires a significantly smaller time step, this corresponds to around 0.4 flow-through times. Overall it took a wall-clock time of 19 and 16 days to perform the single- and two-phase simulations, respectively.

### 3. MODELING

TransAT<sup>®</sup>, which has been used here, is a multi-scale, multi-physics, conservative finite-volume solver for single- and multi-fluid Navier-Stokes equations. The discretization algorithms and schemes employed for pressure-velocity coupling are all high order. In LES the motion of the supergrid turbulent eddies is directly captured, whereas the effect of the smaller scale eddies is modeled. In terms of computational cost, LES [5] lies between RANS and DNS and is motivated by the limitations of each of these approaches. In this work, the subgrid scales were modeled using the wall-adapting local eddy-viscosity (WALE) model. The same value of  $C_s=0.08$  as in [4] was used. Interface tracking was performed using the Level-Set method, with an implicit time-stepping scheme and WENO re-initialization.

### 4. SIMULATION RESULTS

#### 4.1 Single-phase flow, comparison with DNS

Results from the single-phase LES are compared with the DNS performed by Moser et al. [6] to validate the implementation. The mean velocity normalized by the shear velocity is plotted in Figure 3, in both inner and outer scaling. The y-coordinate normalized by  $\nu/u_\tau$  is akin to a local friction Reynolds number. Mean velocity, r.m.s. velocities and Reynolds stresses, see Figure 4, match DNS data very well.

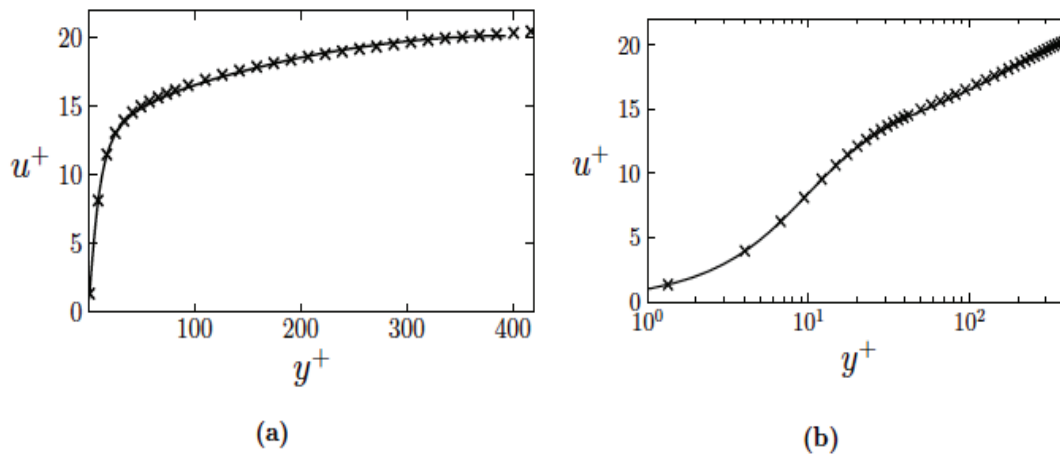


Figure 3: Profiles of mean velocity. Solid line, DNS data [6] at  $Re_\tau = 395$ ; symbols, TransAT LES.

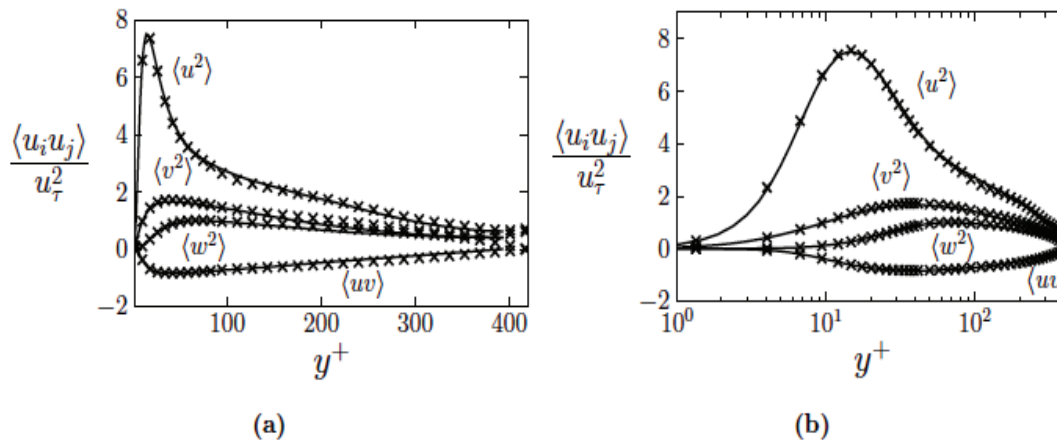
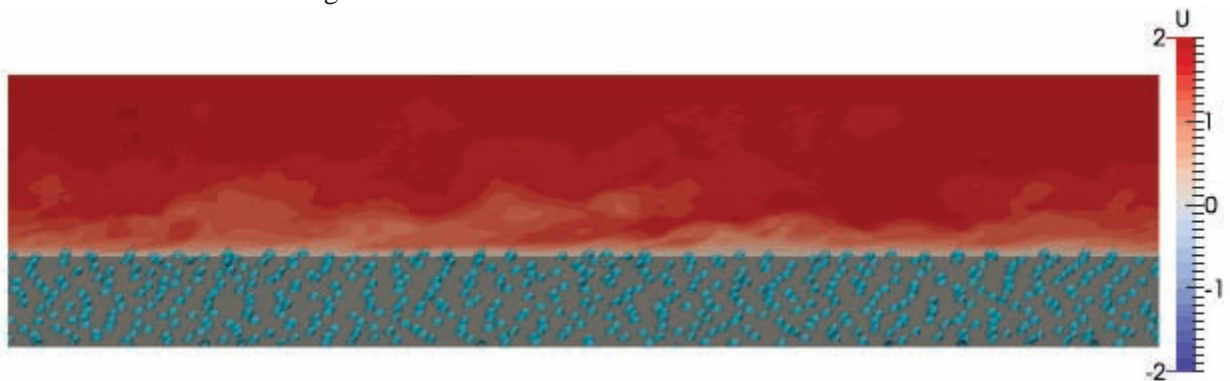


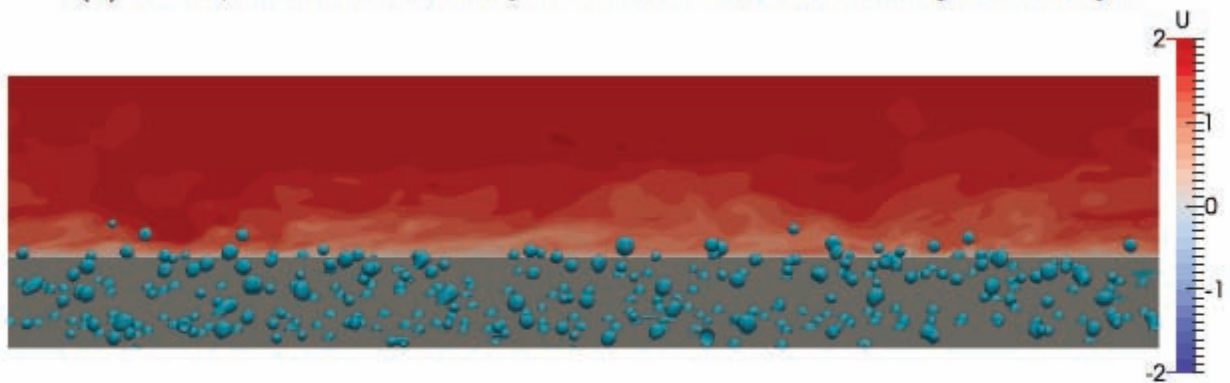
Figure 4: Profiles of the Reynolds stresses. Nomenclature as in Fig. 3.

## 4.2 Near-wall bubbly turbulent channel flow

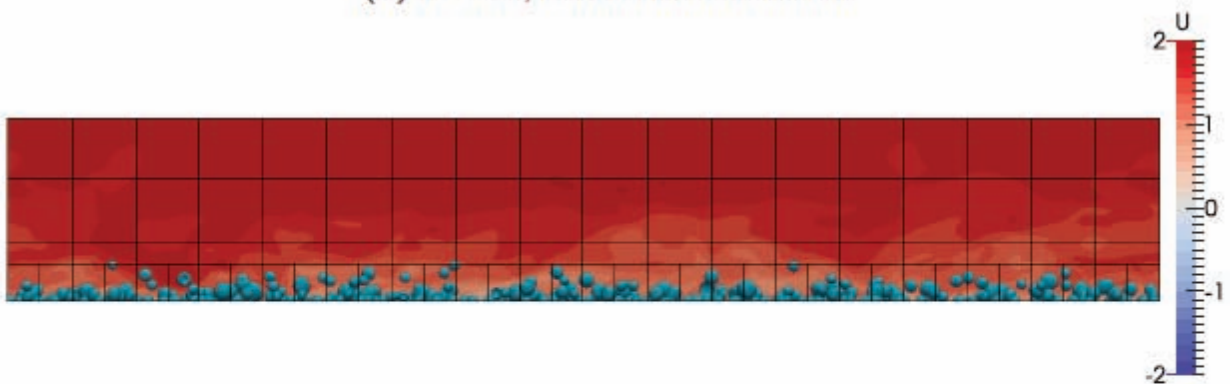
Bubbles are seeded at the wall in the fully developed turbulence. Snapshots from the simulation at different times are shown in Figures 5 and 6.



(a)  $t^+ = 0$ , bubbles are randomly seeded on the wall with hemispherical shape.

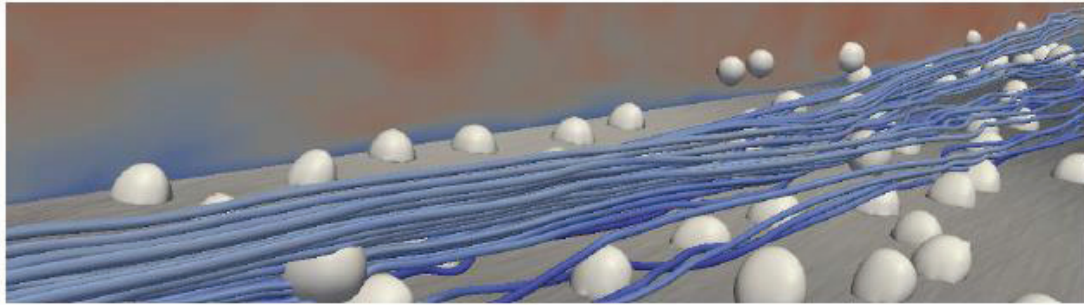


(b)  $t^+ = 59$ , bubbles have detached.

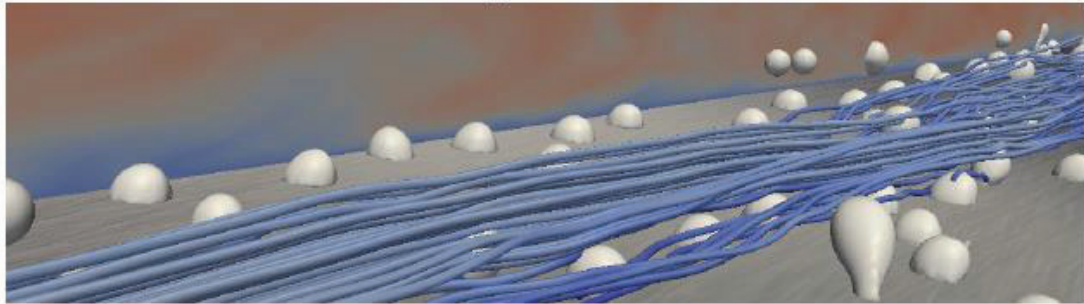


(c)  $t^+ = 59$ , the lines are boundaries between computational blocks used to parallelize the computation. The lowest horizontal line is the boundary between the two BMR regions located at  $y^+ =$ . Bubbles stay in the region refined by the BMR.

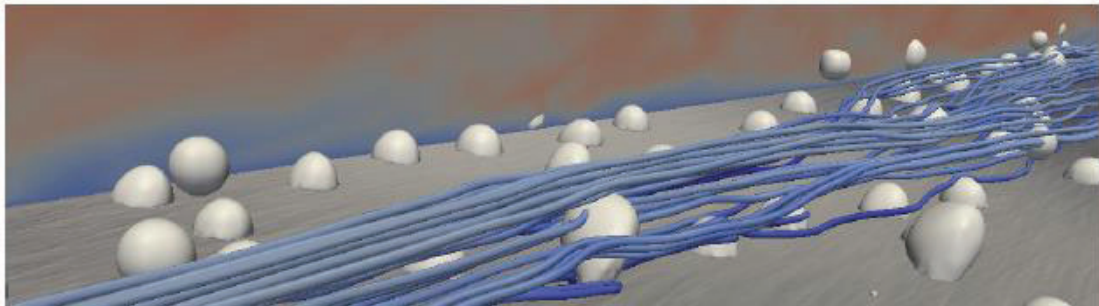
Figure 5: Slice through the domain. The bubbles are colored in blue.



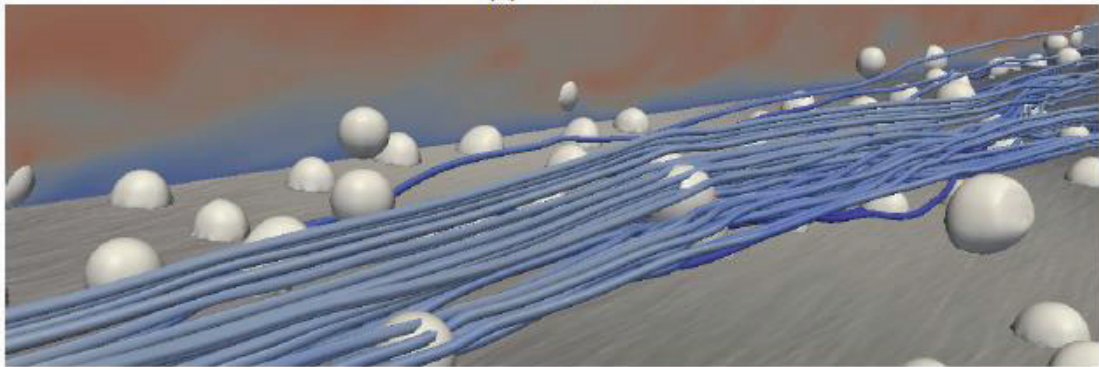
(a)  $t^+ = 20$



(b)  $t^+ = 25$



(c)  $t^+ = 30$



(d)  $t^+ = 35$

Figure 6: Inside view: bubbles detaching from the wall and streamlines.

### 4.3 Velocities and Reynolds stresses in the liquid

We compute the mean velocity and the Reynolds stresses in the liquid to compare the two-phase case with the single-phase one. The near-wall bubbles were found to induce little difference in the mean velocity profile.

The Reynolds stresses are shown in Figures 7-10. The  $\langle u_l'^2 \rangle$  component of the Reynolds stress does not show large differences. However, other Reynolds stresses are largely influenced by the presence of bubbles. The shear Reynolds stress and the spanwise stress both experience an increase of 25% of their maximum values. We also see that the near-wall region has higher Reynolds stresses in the bubbly case. Increase of the Reynolds stresses is particularly significant for the zone occupied by the bubbles  $y^+ < 100$ . From the instantaneous results of the Reynolds stresses, we note that after  $t^+ = 46$  the Reynolds stresses collapse together.

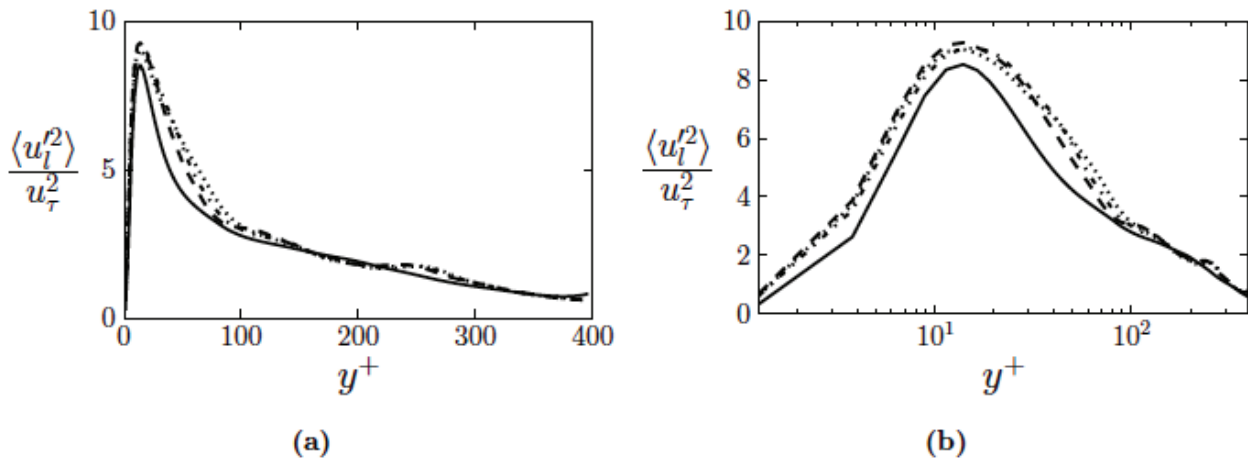


Figure 7:  $\langle u_l'^2 \rangle$  Reynolds stresses: Solid line, single phase; dashed line,  $t^+ = 12$ ; dot-dashed line,  $t^+ = 46$ ; dot line,  $t^+ = 63$ .

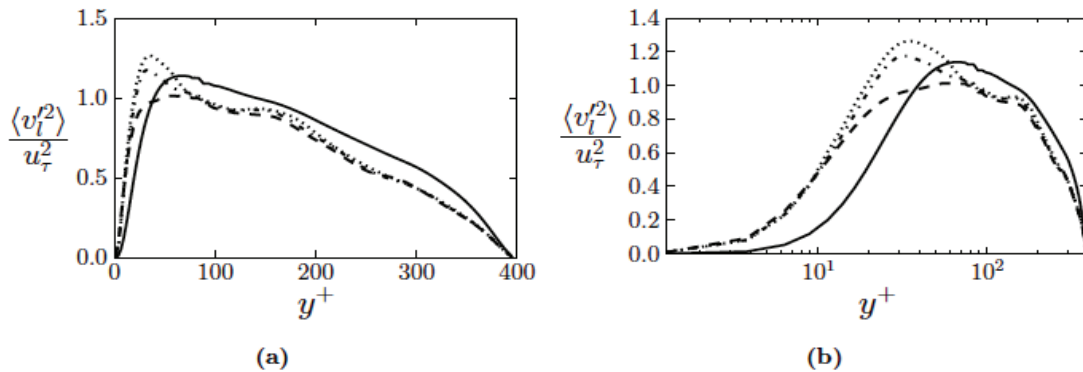


Figure 8: Wall-normal stress: Solid line, single phase ; dashed line,  $t^+ = 12$ ; dot-dashed line,  $t^+ = 46$ ; dotted line,  $t^+ = 63$ .

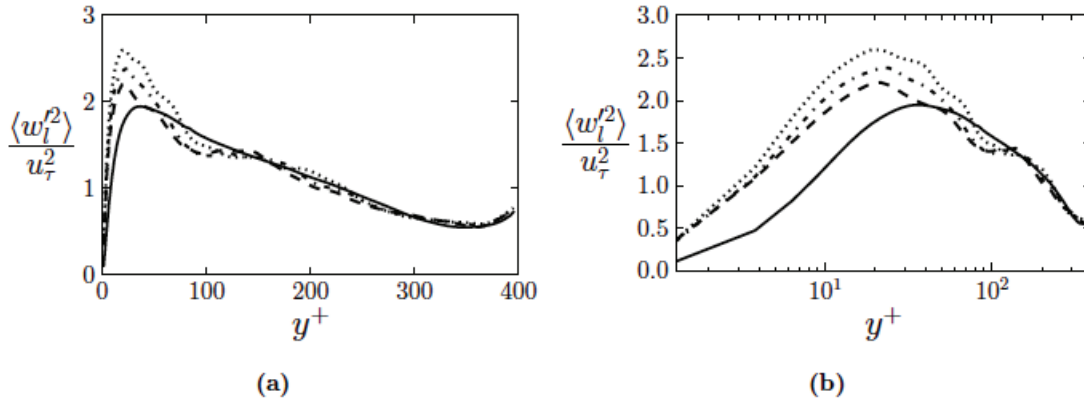


Figure 9: Spanwise stress: Solid line, single phase ; dashed line,  $t^+ = 12$ ; dot- dashed line,  $t^+ = 46$ ; dotted line,  $t^+ = 63$ .

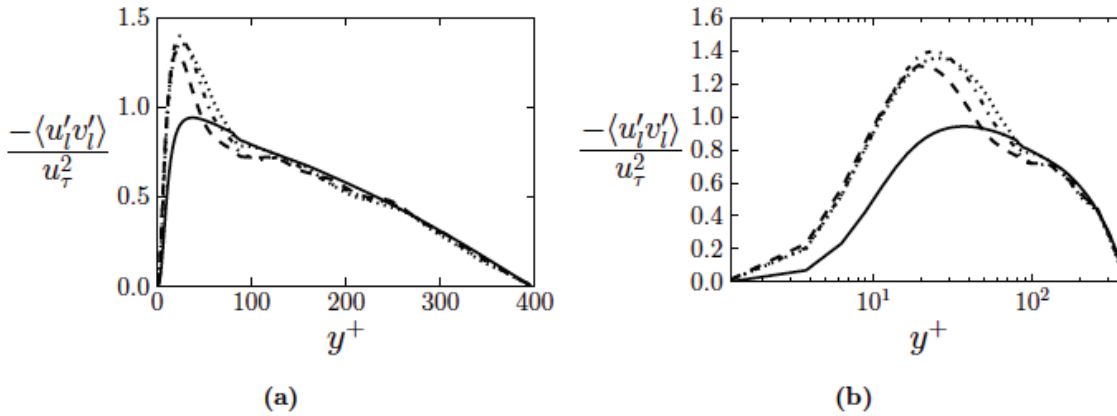
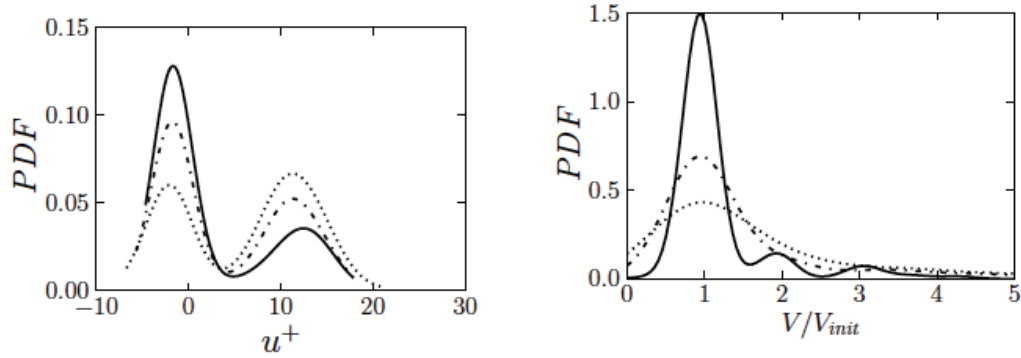


Figure 10: Reynolds shear stress: Solid line, single phase; dashed line,  $t^+ = 12$ ; dot- dashed line,  $t^+ = 46$ ; dotted line,  $t^+ = 63$ .

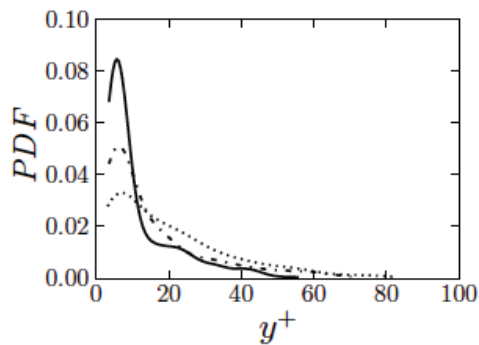
#### 4.4 Bubbles statistics

In this subsection, the focus is put on the dynamics of each individual bubble. The level set method is a Eulerian-Eulerian method. For post-processing, on the other hand, we compute statistics in a Lagrangian way. The final goal is to collect information for each bubble. We derive a procedure to compute mean velocities, volume and center of mass. The path followed by each bubble is also reconstructed.

The probability density functions (PDF) of the velocity, volume and elevation of center of mass of the bubbles are estimated by a kernel density estimation (KDE). The PDF are plotted for three times  $t^+ = 30, 50$  and  $63$  in Figure 11. At  $t^+ = 30$ , a large portion of the bubble population has a velocity close to zero. Approximately all bubbles have volume corresponding to  $V_{init} = 4/3\pi r_b^3$ . As the simulation time increases a peak in the velocity distribution is created at  $u^+ \approx 12$ . Detachment of the bubbles is also shown by the distribution of the center of mass. We see that the bubbles stay in the region refined by the BMR.



(a) PDF of the normalized velocity of the bubbles. (b) PDF of the volume of the bubbles normalized by the volume of sphere of diameter  $D = D_b$ .



(c) PDF of the elevation of the centre of mass of the bubbles.

Figure 11: Bubbles statistics: Solid line,  $t^+ = 30$ ; dot-dashed line,  $t^+ = 50$ ; dot line,  $t^+ = 63$ .

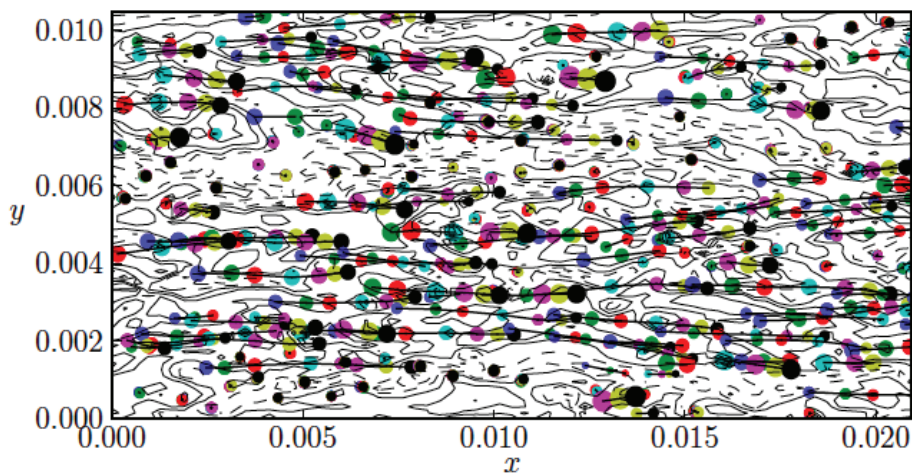


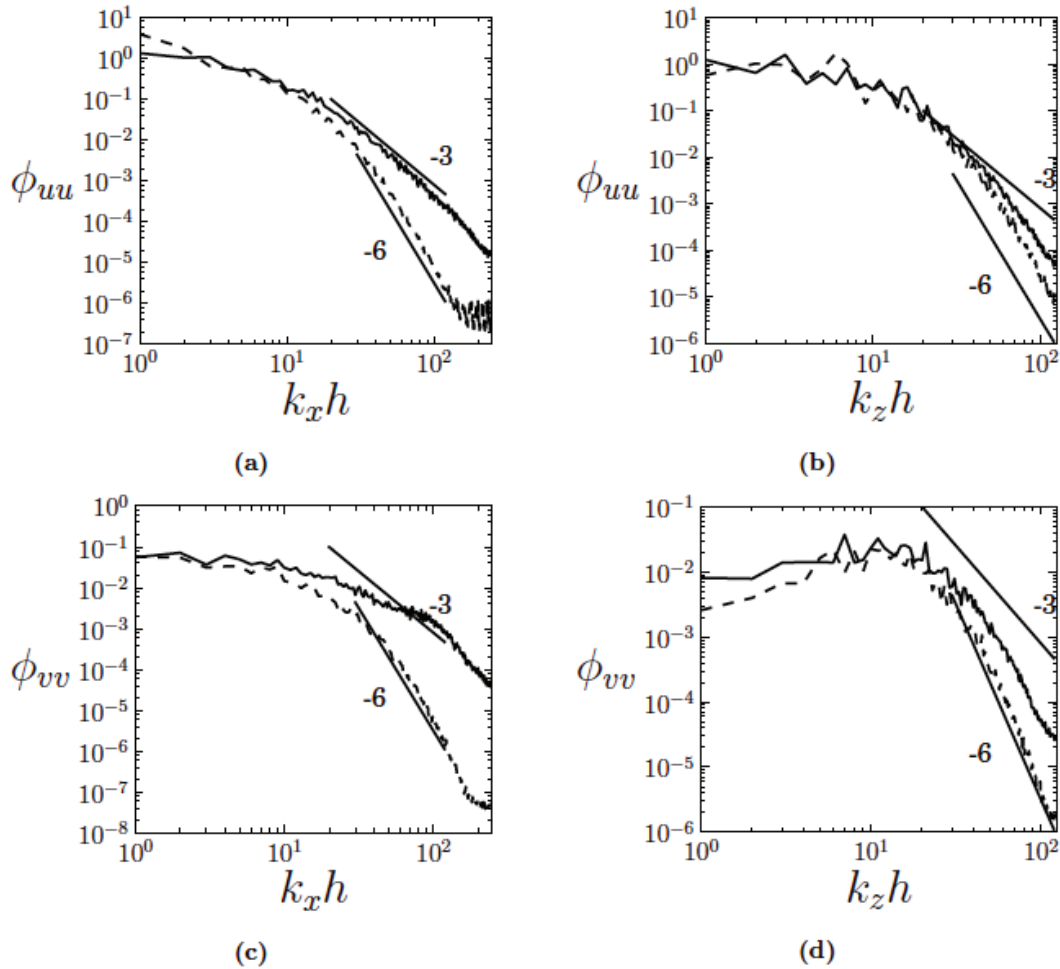
Figure 12: Bubbles path. Blue :  $t^+ = 30$ ; green:  $t^+ = 37$ ; red:  $t^+ = 42$ ; cyan:  $t^+ = 50$ ; magenta:  $t^+ = 55$ ; yellow:  $t^+ = 60$ ; black  $t^+ = 64$ .

## 4.5 Bubbles detachment

Bubbles experience different behaviors depending on their initial location: those initialized in slow regions tend to remain stuck to the wall. Figure 12 shows the location of the bubbles at different times. The diameters of the circles are proportional to the bubble volume. The iso-contours show the value of the instantaneous u-velocity. Dashed lines are the values smaller the mean value in the plane  $y^+ = 20$ .

## 4.6 Velocity spectra

For isotropic turbulence, the inertial subrange exhibits power-law behavior with a  $-5/3$  slope. This is no longer the case for wall-bounded turbulence, where the slope in the inertial subrange depends on the distance to the wall. Velocity spectra are shown direction in Figure 13 for the three velocities on various  $y^+$  planes in x and z. Velocity spectrum is normalized by  $u_\tau^2/h$ . The velocity spectra show relatively large difference between bubbly simulation and single-phase case. The bubbly flow spectra are closer to those found in isotropic flows, indicating that the presence of the bubbles tends to mitigate the anisotropy induced by the wall. For planes further away from the wall the differences between single-phase case and bubbly case decrease, principally because the simulation time was not sufficient for the effects of the bubbles to affect high-order turbulent statistics across the whole height of the channel.



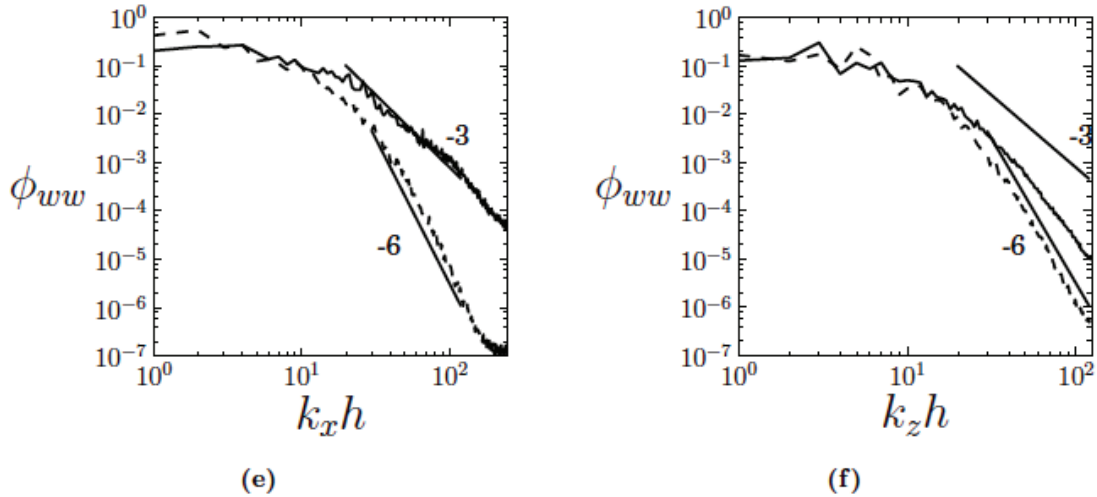


Figure 13: Velocity spectra at  $y^+ = 20$ . Solid line, bubbly case; dashed line, single-phase case.

## 5. CONCLUSIONS

The paper reports a detailed LES-based analysis of turbulent convective flow upward along the heated rods of a PWR sub-channel using the code TransAT. The curvature of the rods was neglected and a configuration of turbulent flow over a flat wall was simulated instead.

A fully developed turbulent velocity field at  $Re = 400$  was used to initialize a two-phase flow simulation where bubbles were seeded on the channel wall. This work is restricted to near-wall turbulent bubbly flow neglecting phase change. No specific models were used for bubble breakup and coalescence.

In contrast with some previous bubbly flow DNS (e.g. [7]), this study puts emphasis on the transient capillary interactions between the bubbles and the wall, as is the case in nucleate boiling. About 600 bubbles are initially adhering to a wall in a flow field where turbulence is already developed. After a short time, bubbles detach and are transported by the flow in close proximity to the wall. Turbulence statistics reach a quasi-steady state but bubbles keep on detaching. About 50% of the bubbles are still adhering to the wall at the end of the simulation.

The interfacial motion of the bubbles is captured explicitly using the Level-Set method. A very fine mesh has to be used in order to resolve the interfacial length scale, leading to a computational domain with 30 millions cells. With this high resolution the LES is actually very close to a Direct Numerical Simulation (DNS) for the turbulent flow scales. This was confirmed by a LES/DNS comparison of a single-phase flow with the same setup.

The presence of bubbles was shown to largely alter the flow variables and. A rapid increase of the wall shear stress at early stage of the simulations and decrease of the anisotropy in the region populated by the bubbles has been observed. The database is now available for use to address RANS models. Boiling heat transfer is addressed in a companion paper.

## 6. ACKNOWLEDGEMENTS

This work has been accomplished in the frame of the FP7 project NURESAFE under grant agreement no 323263. ASCOMP acknowledges PRACE for awarding access to resource Hermit based in Germany at HLRS.

## 7. REFERENCES

- [1] B. Phillips, J. Buongiorno and T. McKrell. 'Nucleation site density, bubble departure diameter, wait time and local temperature distribution in subcooled flow boiling of water at atmospheric pressure, as measured by synchronized high-speed video and infrared thermography', Proc. NURETH 15, Pisa, May 12-15 (2013)
- [2] A. Ashrafian , H.I. Andersson, M. Manhart. 'DNS of turbulent flow in a rodroughened channel'. *Int. J. Heat Fluid Flow* 25 (3), 373–383. (2004)
- [3] P.-Å. Krogstad et al. 'An experimental and numerical study of channel flow with rough walls'. *J. Fluid Mech.* 530, 327–352 (2005)
- [4] D. Chatzikyriakou, J. Buongiorno, D. Caviezel, D. Lakehal. 'DNS and LES of turbulent flow in a closed channel featuring a pattern of hemispherical roughness elements', *International Journal of Heat and Fluid Flow* 53, 29–43 (2015)
- [5] P. Sagaut. 'Large Eddy Simulation for Incompressible Flows', Springer Verlag (2006)
- [6] R. D. Moser, J. Kim, & N. N. Mansour. 'Direct numerical simulation of turbulent channel flow up to  $Re= 590$ '. *Phys. Fluids*, 11(4), 943-945 (1999).
- [7] G. Tryggvason, J. Lu. 'DNS for multiphase flow model generation and validation', Proc. NURETH14, Toronto, Sept. 25-30 (2011).